In situ monitoring of the electrochemical reactivity of aluminium alloy AA6060 using the scanning vibrating electrode technique

J. Izquierdo[1], B.M. Fernández-Pérez[1], J.J. Santana[2], S. González[1,3], R.M. Souto[1,3,*]

[1] Department of Physical Chemistry, University of La Laguna, E-38205 La Laguna (Tenerife, Canary Islands), Spain

[2] Department of Process Engineering, University of Las Palmas de Gran Canaria, Campus Universitario de Tafira, E-35017 Las Palmas de Gran Canaria (Gran Canaria, Canary Islands), Spain.

[3] Instituto Universitario de Materiales y Nanotecnologías, University of La Laguna, E-38200 La Laguna (Tenerife, Canary Islands), Spain

Abstract

Localized electrochemical activation of aluminium alloy AA6060 surfaces during immersion in chloride-containing aqueous solution has been characterised using the scanning vibrating electrode technique (SVET). Ionic current flows in the electrolyte phase adjacent to corroding microcells are imaged *in situ*, allowing their evolution with time to be monitored with spatial resolution. A heterogeneous response due to the presence of intermetallic inclusions in the material is found on AA6060 surfaces. The highly localized anodic activity was thus detected, which has been interpreted as a result of the galvanic coupling between the matrix and the intermetallic particles. Metallic inclusions behave cathodically whereas the aluminium matrix undergoes metal dissolution due to the activation of anodic sites in the proximity of those inclusions. Hydrolysis of aluminium ions leads to local acidification of the electrolyte adjacent to the anodic sites, and it is accompanied by hydrogen evolution.

Keywords: scanning microelectrochemical techniques; SVET; distribution of interfacial electrochemical activity; localized corrosion; aluminium alloy; intermetallic particles.

1. Introduction

The wide use of aluminium and its alloys in a variety of applications arises from the combination of high strength and low density [1], while exhibiting a good corrosion resistance due to the development of a protective oxide layer. However, aluminium alloys are susceptible to localized corrosion in a variety of environments, particularly when chloride ions are present [2-4]. Though pitting corrosion in aluminium-based materials is a complex process that is affected by diverse environmental factors, the composition and microstructure of the alloy surfaces have also been found to significantly influence it [5-7]. The development of microgalvanic differences between the aluminium matrix and the alloying elements would then trigger the corrosion process, leading to localized distributions of corroding sites on the surface of the material [6]. Since most metallic inclusions are nobler than aluminium, they are expected to behave as local cathodes and subsequently induce the anodic dissolution of the metal around them [8-12]. Yet other metals such as Cu, Mg and Zn are less noble than pure aluminium and behave anodically, whereas the aluminium matrix might remain inert while acting as the cathode in the galvanic reaction [1,13-15]. Localized corrosion would also occur in this case, though leading to the removal of active inclusions from the exposed surface of the metal.

Scanning microelectrochemical techniques are increasingly employed to investigate the reactions occurring in corroding systems with high spatial resolution as to gain new insights into the mechanism of the participating reactions [16,17]. Among them, the scanning vibrating electrode technique (SVET) senses potential gradients in the electrolyte phase adjacent to the corroding surface with a high sensitivity [18]. In this way, distributions of microanodes and microcathodes related to localized corrosion processes can be detected *in situ*. Furthermore, the non-destructive character of the technique allows monitoring the time evolution of the systems, independently from the corrosion reactions either undergoing increased dissolution or progressively ceasing as the result of inhibitor action and/or corrosion products precipitation. In this work we have employed SVET to spatially-resolve local differences in electrochemical activity on aluminium alloy AA6060 related to the anodic dissolution of the matrix when exposed to chloride-containing aqueous solution.

2. Experimental

2.1. Samples and solutions

Experiments were carried out on AA6060 wires of diameter 3.2 mm. The composition of the alloy is given in Table 1. The wires were mounted into an epoxy resin sleeve such that only the 3.2 mm diameter circular end surface was free, forming the test metal substrates. The surface of the samples was abraded with SiC paper up to grit 4000. The resulting surfaces were degreased with acetone, abundantly rinsed with ultra-pure deionised water and allowed to dry in air. They were mounted facing up in the electrochemical cell, and immersed in 0.05 M NaCl solution as test media. Solutions were prepared with analytical grade reagents and ultra-pure water purified with a Milli-Q system from Millipore.

2.2. Electrodes and instrumentation

The set-up for microelectrochemical measurements was produced as it follows. The epoxy-sleeved metal specimen (diameter of ca. 4 cm), once polished and cleaned, was taken as the base for the electrochemical cell by placing it horizontally with the polished surface facing upwards. Then the specimen was surrounded laterally by Sellotape, thus allowing a volume for the electrolyte to be filled in.

The scanning vibrating electrode instrumentation was manufactured by Applicable Electronics Inc. (Forestdale, MA, USA) and controlled by dedicated software (Science Wares, Falmouth, MA, USA). A Micro Probe PI200101F microelectrode, which consisted of Pt/Ir (80%/20%) wires insulated with paralene C® and arced at the tip to expose the metal, was employed. The microelectrode was platinized in order to produce a spherical platinum black deposit of 10-20 μm diameter. The measurements were made with the electrode tip vibrating in a plane perpendicular to the sample, at an amplitude of 20 μm and with frequencies in the order of 200-400 Hz. A reference measurement with the microelectrode away from the active area was subtracted from the values measured during the scan. The electrochemical cell was completed by using a Pt-black wire as reference electrode. All the experiments were carried out at the free corrosion potential. A video camera connected to an optical microscope was introduced in the system to follow the movement of the vibrating electrode over the sample during operation as well as to establish the mean distance between the microelectrode and the sample surface. Additionally, changes in the exposed surface as result of the degradation reactions could be monitored by taking photographs just before and after each scan.

3. Results and discussion

Testing of the samples with the SVET technique was carried out on the abraded surfaces immediately following their immersion in the test solution. The development of electrochemical activity on the surface could be monitored by recording the current densities flowing in the solution. In this study, 2D maps were recorded by shifting the vibrating probe at constant height over the sample while the probe was vibrating perpendicular to the substrate. An example of the local current density maps which arise from electrochemical activation of the alloy in 0.05 M NaCl solution is shown in Figure 1. Additionally, micrographs showing the state condition of the explored surface just before and after recording the corresponding SVET map are also given. The actual scanned area has been marked by drawing a blue parallelogram on the photographs.

Figure 1

The activation of localized sites on the metal surface for metal dissolution appears as two local microanodes in the SVET image, whereas the cathodic activity is mainly concentrated in areas close to the anodic sites. It must also be noticed that the electrochemical activity at the anodes is quite different for the two sites monitored in this map. Ionic currents 2-3 times bigger occurred at the microanode found in the upper half of the image, which may be an indication of an independent development of electrochemical activity at each site with the elapse of time. The evolution of gas bubbles from the surface is also observed from inspection of the micrographs.

The time evolution of electrochemical activity on the surface was next monitored by recording a series of SVET maps at different elapsed times since immersion of the sample in the electrolyte. Smaller areas were scanned to reduce the time required for the acquisition of the maps. Figure 2 shows the SVET images and the micrographs of the scanned area obtained for the sample during 4 hours immersion in 0.05 M NaCl. Localization of reacting sites is observed at all times, though they are found to shift position on the surface, supporting that these sites are progressively activated and subsequently deactivated during the exposure to the aggressive environment. Inspection of the micrographs in Figure 2 allowed us to observe that corrosion products were deposited in those sites at which electrochemical activity occurred at earlier exposures.

Figure 2

Gas evolution was located at the anodic sites. Bubbles were often removed during the passage of the vibrating probe over the scanned substrate and thus they could not be usually observed in the micrographs taken just after recording the SVET images. Yet the active site remained

producing gas evolution, and a new bubble might eventually become visible in the optical microscope as shown in Figure 3.

Figure 3

The observed features can be justified by considering the nucleation of corroding pits on the surface of the alloy, at which protons can be formed during the hydrolysis of metal ions released from the corroding anodic sites.

$$Al^{3+} + 2\ H_2O \rightarrow Al(OH)_2^{+} + 2\ H^{+} \qquad (1)$$

This reaction would also involve the formation of hydroxide species which may eventually lead to the precipitation of corrosion products. These compounds may either block the opening of the corroding pit or lead to the repassivation of the corroding site after some time.

The combination of a low pH around the anodic sites and a sufficiently negative mixed potential for the alloy immersed in the electrolyte are sufficient for hydrogen evolution reaction to occur from the anodic sites, similarly to the so-called “anomalous hydrogen evolution” effect described during the corrosion of magnesium and its alloys in aqueous environments [19]. Thus, only a fraction of the released protons can diffuse into the electrolyte, and it is detected by the SVET as a positive ionic current flowing from the pit. Outside the pit, the media is not acidic, so the reduction half reaction is still oxygen reduction because the medium is not acidic. In the latter case, the formation of hydroxide ions is detected as a negative ionic current.

This passivation effect was further investigated by treating a sample in the following way. The sample was firstly immersed in 0.05 M NaCl for 24 hours. Upon removal from the solution, the complete surface of the alloy in the sample was covered by a black film layer considered to be formed by corrosion products. Subsequently, a portion of the surface was abraded to remove this precipitate layer, and it was then carefully cleaned with distilled water in order to not modify the remaining non-abraded surface of the alloy (see Figure 4 for a sketch of the substrate). The resulting substrate was introduced again in 0.05 M NaCl solution, and a series of SVET images were recorded by scanning the vibrating probe over both the abraded and the non-abraded portions of the surface. In this way, the time evolution of the substrate with two different surface finishes could be monitored in situ.

SVET images were recorded over a period of 21 hours after immersion of the sample in the test electrolyte. Figure 5 shows selected SVET images and optical micrographs taken just before the maps were actually recorded. At all times, the active anodic sites were found in the abraded portion

of the sample, thus confirming the passive state achieved by the surface alloy in the test electrolyte at long exposures. Therefore, we regard the corrosion reaction of alloy AA6060 exposed to chloride-containing environments to involve the formation of corroding pits which may eventually be passivated through a precipitation mechanism, and the process is subsequently initiated at a different location. The formation of pits could also be confirmed from the inspection of retrieved samples under a microscope, as shown in Figure 6.

Figure 5

Figure 6

Oxidation of the aluminium matrix would imply the occurrence of metallic inclusions that behave cathodically as described in the sketch depicted in Figure 7. This behaviour can be expected for either Al(CuMnFe) or Al(MnSi) inclusions. In this case, the extent of the surrounding aluminium matrix undergoing oxidative dissolution processes has been proposed to be approximately 5 times greater than the cathodic sites (i.e., 200 – 250 μm) [20], and they could be monitored using SVET. When protons are the chemical species reduced at the microcathodes, evolution of hydrogen gas occurs on the alloy surface.

Figure 7

The microgalvanic mechanism also serves to describe the observed differences in time evolution of the corrosive process as monitored by SVET in terms of the microstructure and composition of the alloy. High strength aluminium alloys like AA6060 and AA2024 (Al-4.4Cu-1.5Mg-0.6Mn) are microstructurally complex materials presenting various individual phases that greatly influence the corrosion behaviour. Though nucleation of corrosion pits occur on AA6060 as well as on AA2024 aluminium alloys, despite their different composition and distribution of repassivation of the pits only occurs for the former, thus leading to the progressive displacement of anodic and cathodic sites over the surface with the elapse of time. Conversely, such repassivation process does not occur on the AA2024 alloy [21], and the dissolution process at the anodic sites continue progressing with time [21,22], probably due to self corrosion of the aluminium matrix via hydrogen evolution, leading to significantly higher corrosion rates for this alloy.

4. Conclusion

The occurrence of localized electrochemical activation of complex systems such as aluminium alloys can be monitored using the scanning vibrating electrode technique (SVET) when

the samples are immersed in an electrolytic corroding environment. The sizes of the anodic and cathodic sites observed in our work are much bigger than those typically corresponding to metallic inclusions in the alloy (namely, 20-50 μm), a feature that must be taken in account for mechanistic considerations.

Oxidation of the aluminium matrix would imply the occurrence of metallic inclusions that behave cathodically whereas the surrounding aluminium matrix undergoes oxidative dissolution processes. When protons are the chemical species reduced at the microcathodes, evolution of hydrogen gas occurs on the alloy surface.

Acknowledgments

This publication was made possible by grant No. CTQ2012-36787 from the Spanish Ministry of Economy and Competitiveness (MINECO, Madrid, Spain) and the European Regional Development Fund (Brussels, Belgium). A Research Training Grant awarded to J.I. by the Spanish Ministry of Education (Programa de Formación de Personal Investigador) is gratefully acknowledged.

References

1. F.M. Queiroz, M. Magnani, I. Costa, H.G. de Melo, Investigation of the corrosion behaviour of AA 2024-T3 in low concentrated chloride media, Corrosion Science 50 (2008) 2646-2657.
2. J.B. Bessone, D.R. Salinas, C.E. Mayer Ebert, W.J. Lorenz, An EIS study of aluminium barrier-type oxide films formed in different media, Electrochimica Acta 37 (1992) 2283-2290.
3. A.G. Muñoz, J.B. Bessone, Pitting of aluminium in non-aqueous chloride media, Corrosion Science 41 (1999) 1447-1463.
4. L.C. Abodi, J.A. DeRose, S. Van Damme, A. Demeter, T. Suter, J. Deconinck, Modeling localized aluminum alloy corrosion in chloride solutions under non-equilibrium conditions: Steps toward understanding pitting initiation, Electrochimica Acta 63 (2012) 169-178.
5. A. Alavi, R. Cottis, The determination of pH, potential and chloride concentration in corroding crevices on 304 stainless steel and 7475 aluminium alloy, Corrosion Science 27 (1987) 443-451.
6. K. Nisancioglu, Electrochemical behaviour of aluminium-base intermetallics containing iron, Journal of the Electrochemical Society 137 (1990) 69-77.

7. M. Bethencourt, F.J. Botana, J.J. Calvino, M. Marcos, M.A. Rodriguez, Influence of the surface distribution of Al_6(MnFe) intermetallic on the electrochemical response of AA5083 aluminium alloy in NaCl solutions, Mater Sci Forum 289–292 (1998) 567-574.
8. Z. Szklarska-Smialowska, Pitting corrosion of aluminum, Corrosion Science 41 (1999) 1743-1767.
9. E.V. Koroleva, G.E. Thompson, G. Hollrigl, M. Bloeck, Surface morphological changes of aluminium alloys in alkaline solution: effect of second phase material, Corrosion Science 41 (1999) 1475-1495.
10. P. Campestrini, E.P.M. van Vesting, H.W. van Rooijen, J.H.W. de Wit, Relation between microstructural aspects of AA2024 and its corrosion behaviour investigated using AFM scanning potential technique, Corrosion Science 42 (2000) 1853-1861.
11. N. Birbilis, M.K. Cavanaugh, R.G. Bucheit, Electrochemical behavior and localized corrosion associated with Al_7Cu_2Fe particles in aluminum alloy 7075-T651, Corrosion Science 48 (2006) 4202-4215.
12. R. Grilli, M.A. Baker, J.E. Castle, B. Dunn, J.F. Watts, Localized corrosion of a 2219 aluminium alloy exposed to a 3.5% NaCl solution, Corrosion Science 52 (2010) 2855-2866.
13. P. Campestrini, H.W. van Rooijen, E.P.M. van Vesting, J.H.W. de Wit, Influence of quench delay time on the corrosion behavior of aluminium alloy 2024, Materials and Corrosion 51 (2000) 616 -627.
14. J. Zhang, M. Klasky, B.C. Letellier, The aluminum chemistry and corrosion in alkaline solutions, Journal of Nuclear Materials 384 (2009) 175-189.
15. A.E. Hughes, A. Boag, A.M. Glenn, D. McCulloch, T.H. Muster, C. Ryan, C. Luo, X. Zhou, G.E. Thompson, Corrosion of AA2024-T3. Part II: Co-operative corrosion, Corrosion Science 53 (2011) 27-39.
16. R. Oltra, Local electrochemical methods in corrosion research, in: Local Probe Techniques for Corrosion Research (R. Oltra, V. Maurice, R.Akid, P. Marcus, Eds.); Woodhead Publishing, Cambridge (2007), p. 1-11..
17. M.B. Jensen, D.E. Tallman, Application of SECM to corrosion studies, in: Electroanalytical Chemistry: A Series of Advances, vol. 24 (A.J. Bard, C.G. Zoski, Eds.); CRC Press, Boca Raton (2012), p. 171-286.
18. R.S. Lillard, Scanning electrode techniques for investigating near-surface solution current densities, in: Analytical Methods in Corrosion Science and Engineering (P. Marcus, F. Mansfeld, Eds.); CRC Press, Boca Raton (2006), p. 571-604.

19. G. Song, Recent progress in corrosion and protection of magnesium alloys, Advances in Engineering Materials 7 (2005) 563-586.
20. R.P. Wei, C.-M. Liao, M. Gao, A transmission electron microscopy study of constituent-particle-induced corrosion in 7075-T6 and 2024-T3 aluminum alloys, Metallurgical Materials Transactions A 29 (1998) 1153-1160.
21. R.M. Souto, J. Izquierdo, J.J. Santana, S. González, Scanning microelectrochemical techniques: A highly sensitive route to evaluate degradation reactions and protection methods with chemical selectivity, European Journal of Science and Theology 9 (2013) 71-89.
22. J. Izquierdo, S. González, R.M. Souto, Application of AC-SECM in corrosion science: Local visualization of heterogeneous chemical activity in AA2024 surfaces, International Journal of Electrochemical Science 7 (2012) 11377-11388.

Table 1. Composition of AA6060 aluminium alloy (wt.%)

Al	Balance
Cu	< 0.02
Mg	0.4 – 0.45
Si	0.4 – 0.45
Fe	0.15 – 0.22
Mn	< 0.03
Ti	< 0.02
Cr	< 0.02
Zn	< 0.02
Pb	< 0.02

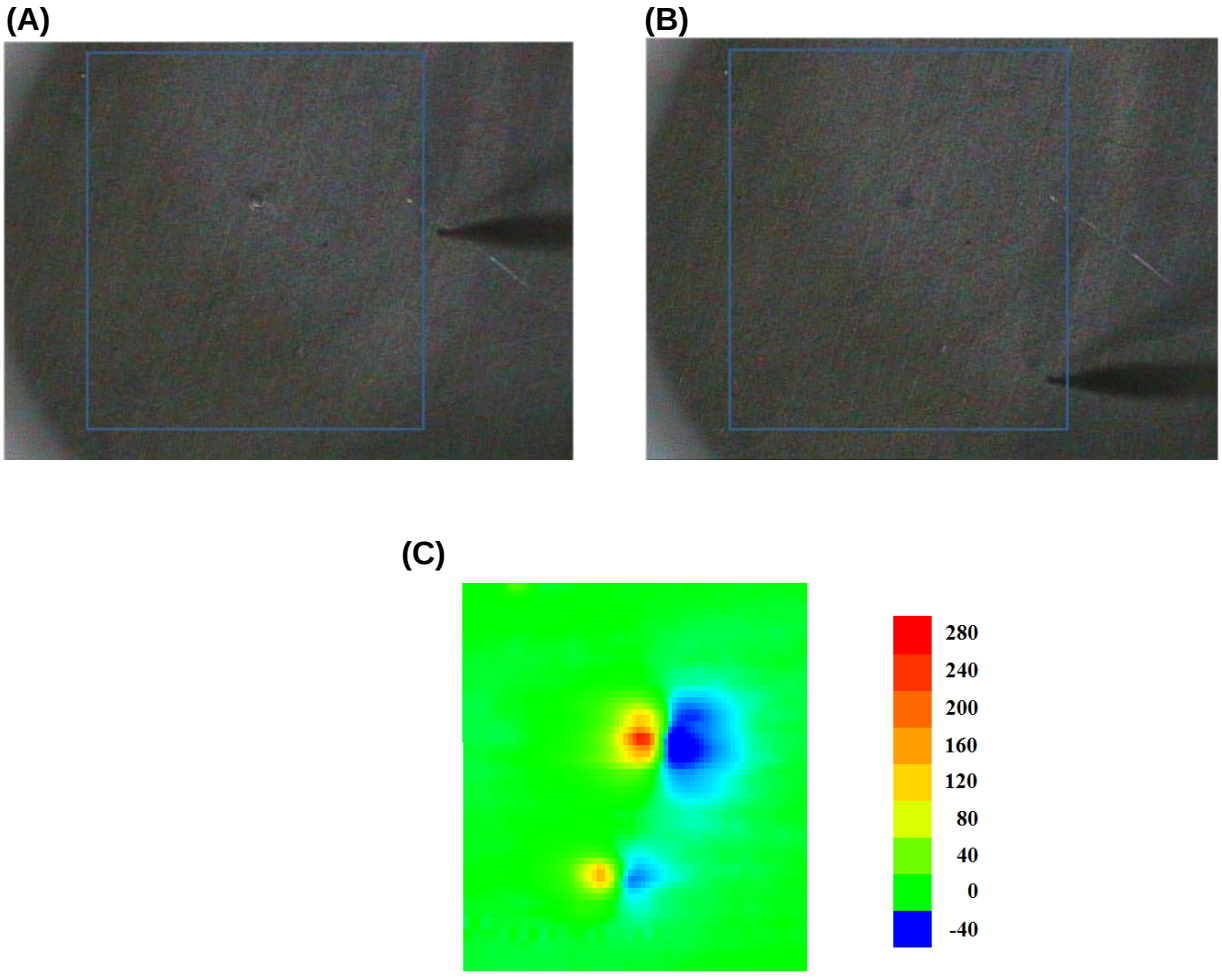

Figure 1. (A, B) Micrographs, and (C) SVET image of AA6060 alloy immersed in 0.05 M NaCl aqueous solution for ca. 20 minutes. The micrographs were taken just (A) before and (B) after recording the SVET image. Values of *Z* axis: Ionic current, μA cm^{-2}. Mean probe-substrate distance: 50 μm. The images represent 2300 μm x 2600 μm in *X* and *Y* directions.

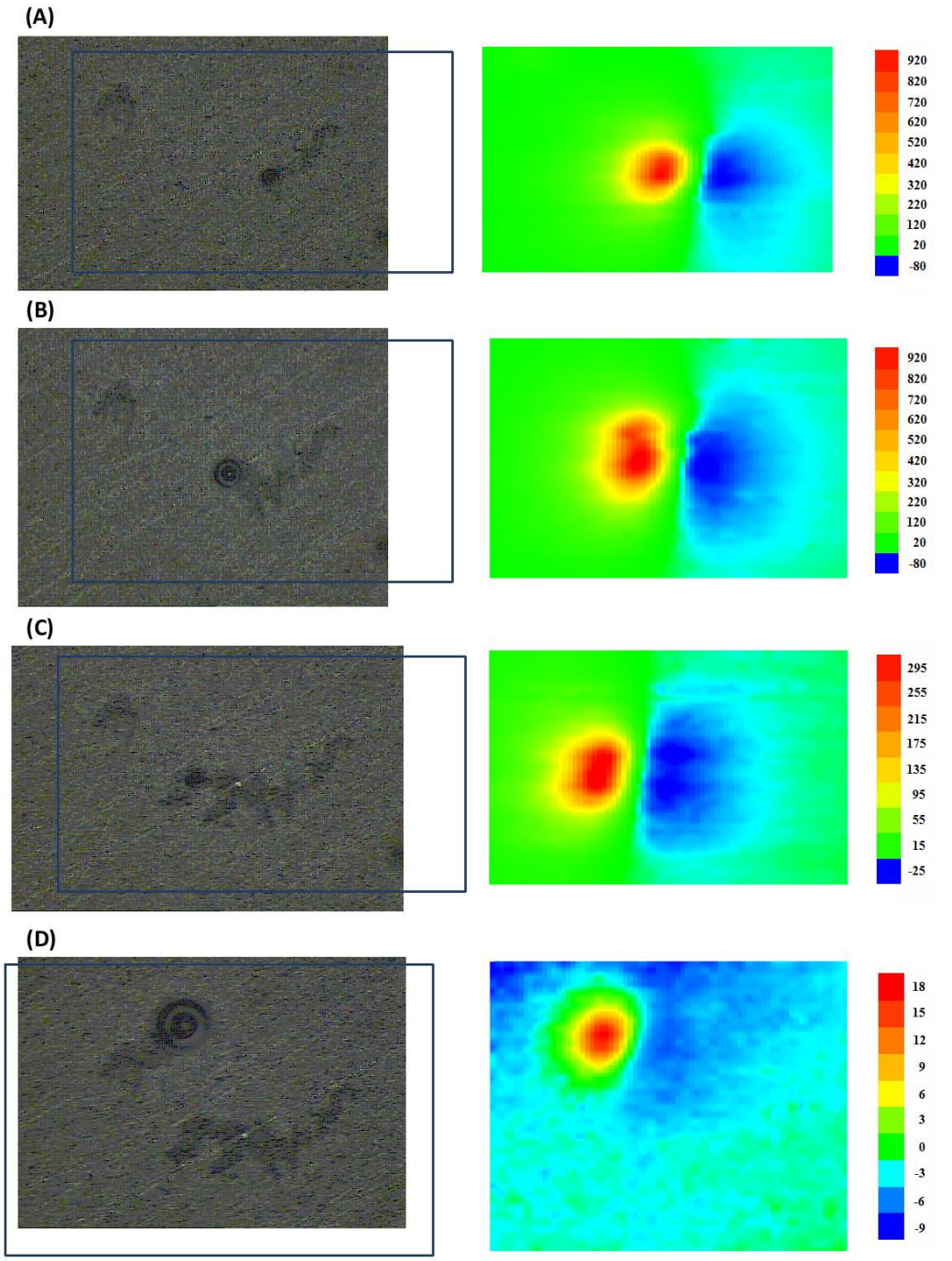

Figure 2. SVET images and micrographs of AA6060 alloy immersed in 0.05 M NaCl aqueous solution for: (A) 95, (B) 125, (C) 170, and (D) 270 minutes. Values of *Z* axis: Ionic current, μA cm^{-2}. Mean probe-substrate distance: 80 μm. The images represent 1500 μm x 1000 μm in *X* and *Y* directions.

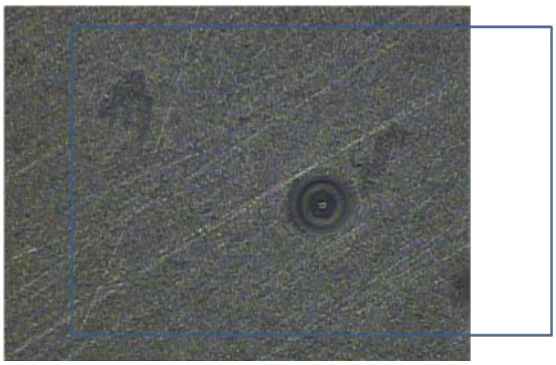

Figure 3. Micrograph of the AA6060 alloy immersed in 0.05 M NaCl aqueous solution taken after the SVET map in Figure 3A was recorded.

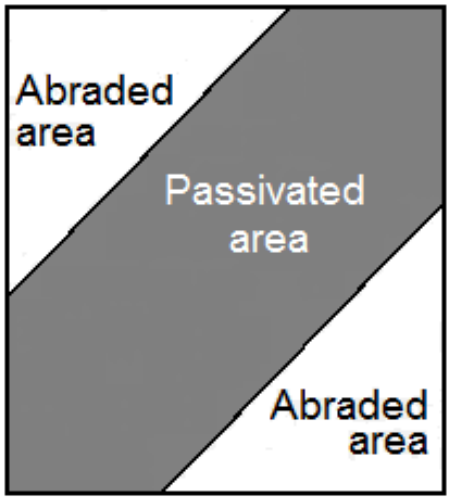

Figure 4. Sketch depicting sample preparation. The sample is corroded for 24 hours in 0.05 M NaCl. After retrieval, two portions of the surface are abraded with 4000 grit emery paper to remove the surface film from the metal sample, leaving an abraded area. The resulting sample is exposed again to 0.05 M NaCl. The surface scanned in order to record the SVET images covers both the abraded and the non-abraded portions of the sample.

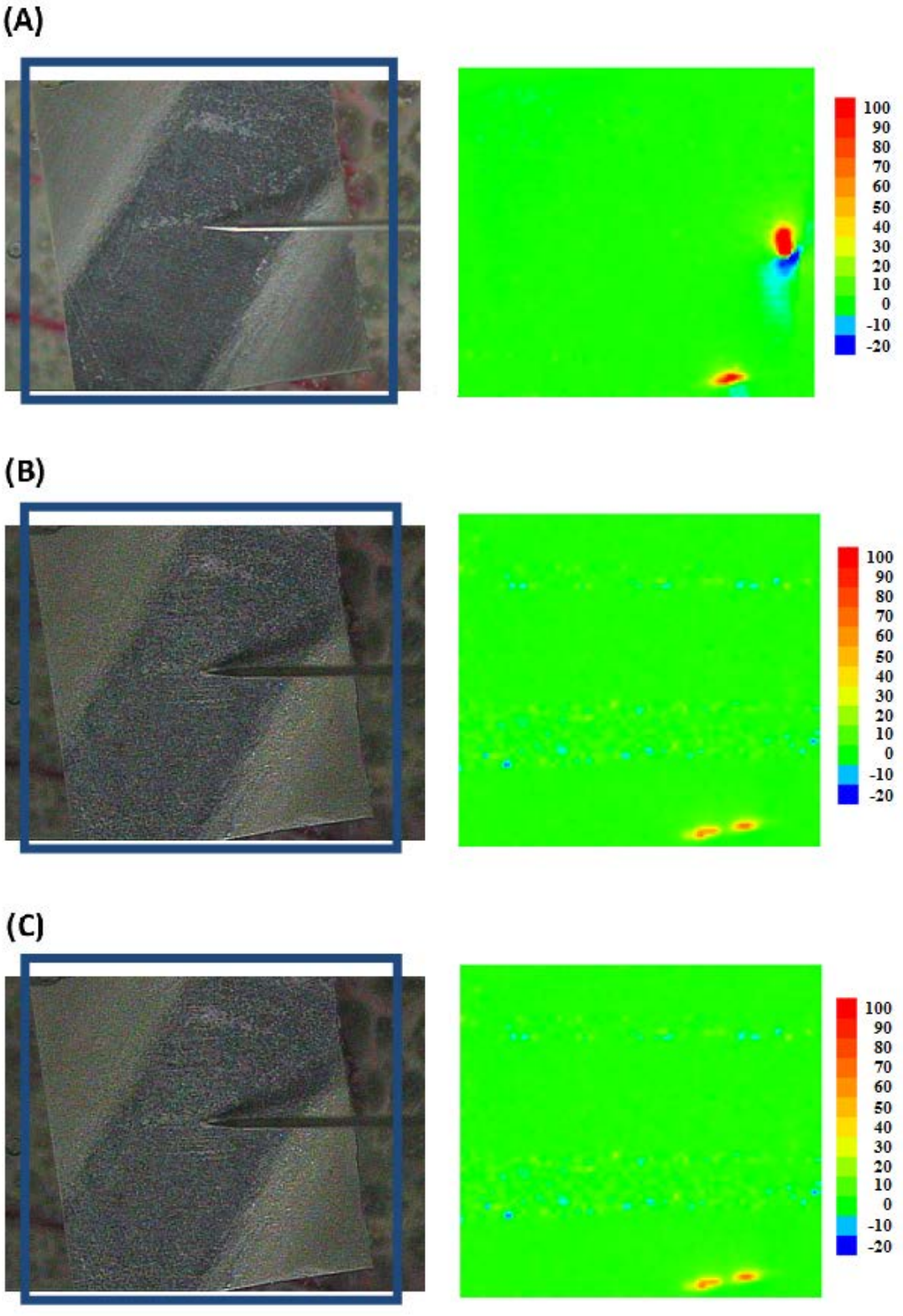

Figure 5. SVET images and micrographs on an abraded – passivated (24 hours treatment in 0.05 M NaCl) AA6060 alloy system (from bottom to top) during immersion in 0.05 M NaCl aqueous solution for: (A) 1, (B) 9, and (C) 21 hours. Values of *Z* axis: Ionic current, μA cm^{-2}. Mean probe-substrate distance: 40 μm. The images represent 1200 μm x 3400 μm in *X* and *Y* directions.

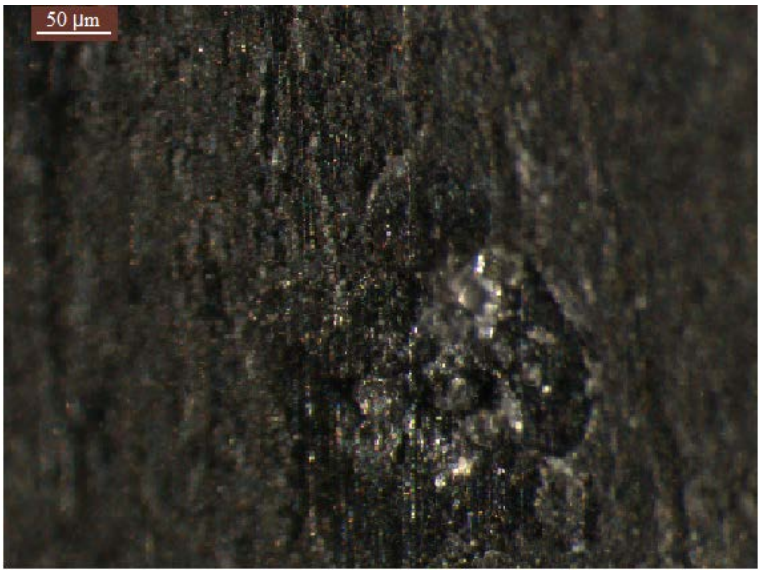

Figure 6. Optical micrograph of a retrieved AA6060 alloy sample after completing the tests described in Figure 6.

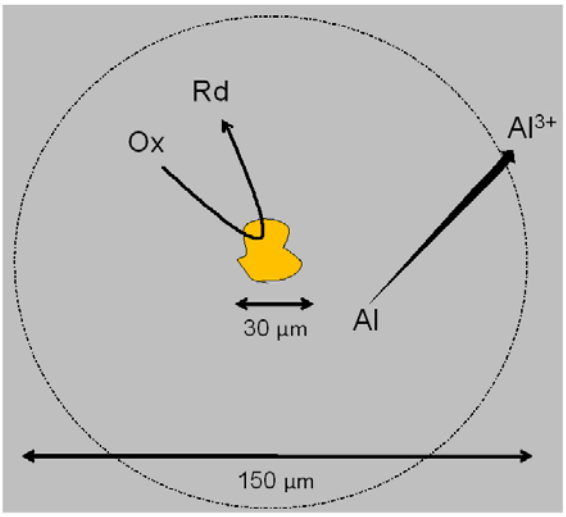

Figure 7. Sketch describing the corrosion process at aluminium alloys sustained by metallic inclusions with a cathodic behaviour.